Electronic Supplementary Information

A strategy for increasing the breakdown field strength beyond the experimental scaling law in yttria films

Tomohiko Nakajima,[*a] Yuuki Kitanaka,[a] Iwao Yamaguchi,[a] Kazuhiro Kumagai [b], Junichi Nomoto [a], Masayuki Fukuda [a] and Ryohei Hokari [a]

[a.]Advanced Manufacturing Research Institute, National Institute of Advanced Industrial Science and Technology, Tsukuba Central 5, 1-1-1 Higashi, Tsukuba, Ibaraki 305-8565, Japan.

[b.]Industrial Cyber-Physical Systems Research Center, National Institute of Advanced Industrial Science and Technology, 10-2 Haruechō Edomekamiyamato, Sakai, Fukui 919-0462 Japan.

Nanoparticle size distribution in the dispersion ink

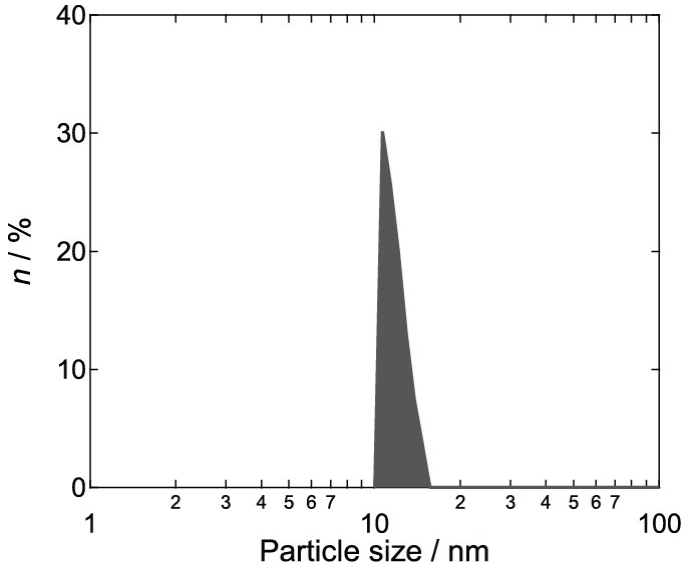

Fig. S1: The particle size dependence of particle number (%) in the prepared yttria nanoparticle dispersion ink.

Table S1 Process conditions and properties of the yttria films.

Process	Thickness / μm	Dielectric strength / MV/cm	Breakdown voltage / kV	Max. Process Temp / °C	Ref.
AD	10	1.57	1.57	25	S1
ALD	0.02	6.1	0.0122	300	S2
ALD	0.06	5.75	0.0345	225	S3
ALD	0.03	5	0.015	280	S4
MOCVD	0.04	8	0.032	450	S5
MOCVD	0.04	8	0.032	350	S6
MOCVD	0.24	1.1	0.0264	600	S7
MOCVD	0.5	2.4	0.12	400	S8
PLD	0.02	6.5	0.013	600	S9
Sputtering	0.017	1.33	0.00227	800	S10
Sputtering	0.13	3.85	0.0501	190	S11
Sputtering	0.0648	1.97	0.0128	300	S12
Sputtering	0.077	4.85	0.0373	200	S12
CSD	0.015	5	0.0075	450	S13
CSD	0.1	3.5	0.035	500	S14
CSD	0.06	5	0.03	400	S15
Plasma Spray	30	0.4	1.2	25	S16
Plasma Spray	100	0.144	1.44	25	S17
Plasma Spray	231	0.167	3.86	25	S18
Plasma Spray	521	0.173	9.01	25	S19
Plasma Spray	554	0.144	7.98	25	S19
Plasma Spray	531	0.116	6.16	25	S19
IBAD	0.318	3.9	0.124	25	S20
EBE	0.1	4	0.04	25	S21
EBE	0.08	2	0.016	625	S22
MBE	0.014	6	0.0084	200	S23
PCSD	0.16	6.45	0.101	400	This work
PCSD	0.37	7.37	0.275	400	This work
PCSD	0.87	12.5	1.09	400	This work
PCSD	1.43	12.7	1.82	400	This work

Transmittance spectrum for the precursor yttria film

The transmittance spectrum for the precursor yttria film before the excimer laser irradiation is shown in Fig. S2. The transparency at 248 nm (KrF) and 193 nm (ArF) were 67.5% and 40.6%, respectively.

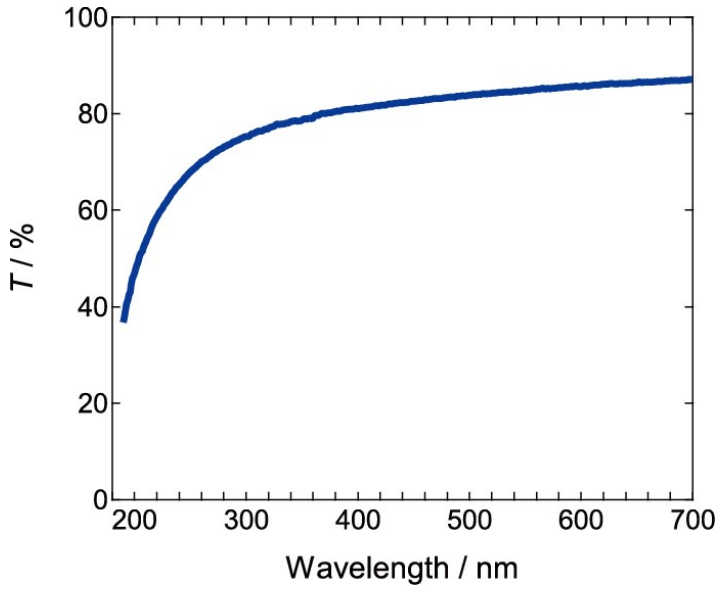

Fig. S2: The transmittance spectrum for the precursor yttria film prepared on a silica glass substrate before the excimer laser irradiation.

Instantaneous photothermal heating simulations for the precursor yttria film

Temperature variations during laser irradiation were simulated by the heat diffusion equation simplified for one-dimensional heat flow:

$$\rho_m C\frac{\partial T}{\partial t} = \kappa\frac{\partial^2 T}{\partial z^2} + \alpha I(z,t) \qquad \text{(E1)}$$

where T is the temperature function at time t and depth z, ρ_m is the mass density, C is the specific heat capacity, α is the optical absorption coefficient, κ is the thermal conductivity, and $I(z,t)$ is the laser power density. The laser power $I(z,t)$ is given by:

$$I(z,t) = I_0(t)\cdot(1-R)\cdot\exp(-\alpha z) \qquad \text{(E2)}$$

where R is the reflectance. In the calculation, a contribution of incremental absorbance for the films due to the reflectance at substrate surface was also included to the laser power distribution. $I_0(t)$ is described as a smooth pulse approximated by:

$$I_0(t) = I_0\cdot\left(\frac{t}{\tau}\right)^{\beta}\cdot\exp\left(\beta\left(1-\frac{t}{\tau}\right)\right) \qquad \text{(E3)}$$

where I_0 is the incident pulse power density, τ is the pulse duration, and β determines the temporal pulse shape. We carried out numerical simulations for the temperature variation for the excimer laser irradiation process using a difference approximation based on the above equations. The boundary conditions used were T = 300 °C at t = 0 s (the initial substrate temperature), T = 300 °C at the bottom of the substrate, and $\kappa(\partial T/\partial z) = 0$ at the interfaces (adiabatic condition). The thermal and physical properties for the numerical simulations are listed in Table S2, according to Refs.

S24 and S25. The properties of precursor Y_2O_3 were partly used in place of crystallized Y_2O_3. It should be noted that this thermal simulation does not account for the heat shielding effect of elliptical pores as air layers, which may result in a quantitative underestimation.[S26] However, this does not affect relative comparisons between KrF and ArF or among different fluences.

Table S2 Thermal and physical properties for the numerical simulations.[S24,S25]

Materials	α (cm^{-1})	R	κ (W cm^{-1}K^{-1})	ρ (g cm^{-3})	C (J g^{-1}K^{-1})
Y_2O_3 (248 nm, KrF)	56148.9	0.08	0.13	4.85	0.456
Y_2O_3 (193 nm, KrF)	128771.7	0.09			

The optical absorption coefficient and reflectance were measured for the precursor film, while the thermal conductivity and specific heat were obtained from literature values for the crystalline phase. The density was calculated based on the theoretical density, adjusted for the measured porosity.

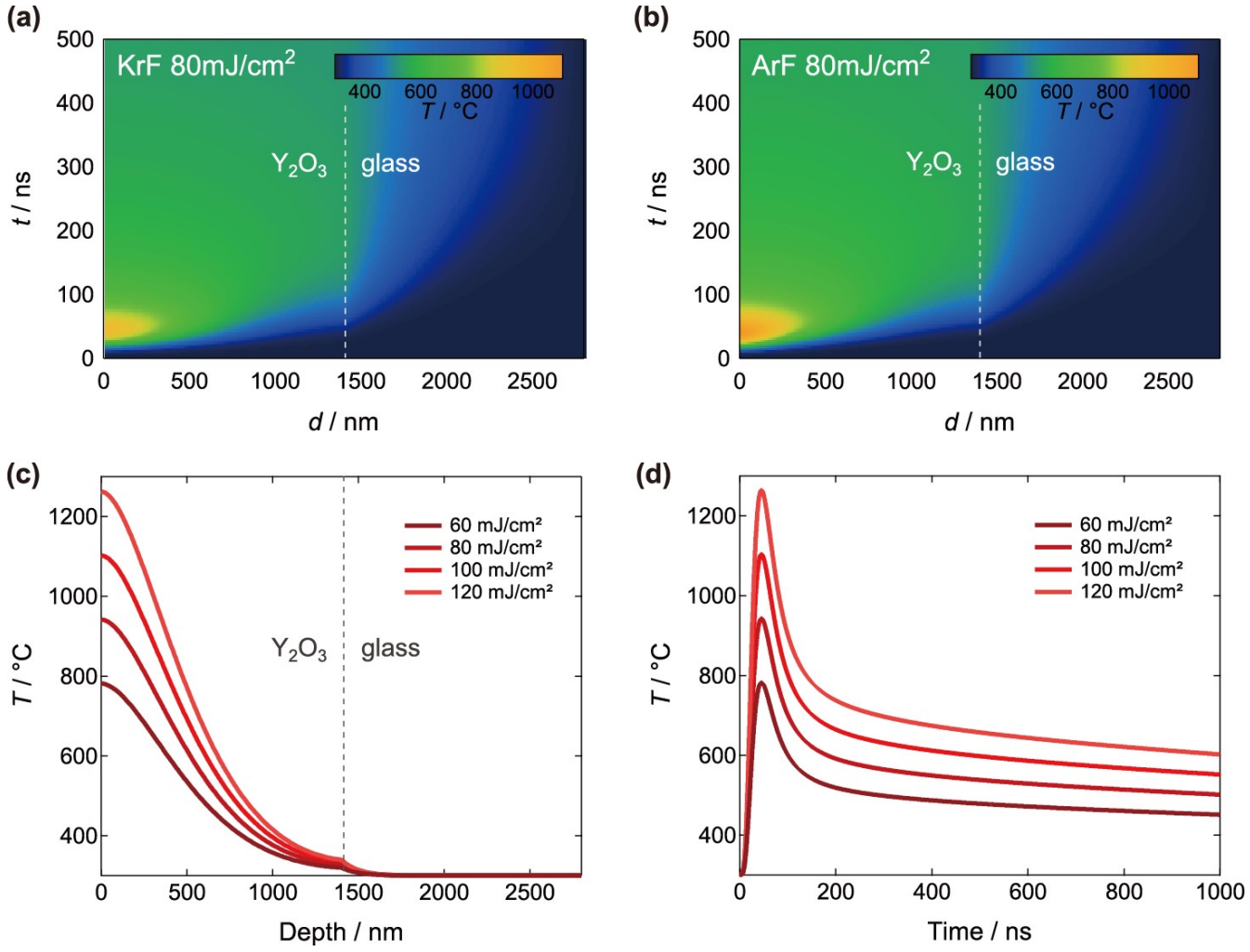

Fig. S3: The transmittance spectrum for the precursor yttria film prepared on a silica glass substrate before the excimer laser irradiation.

Elliptical pore formation and densification during the multiple coating process

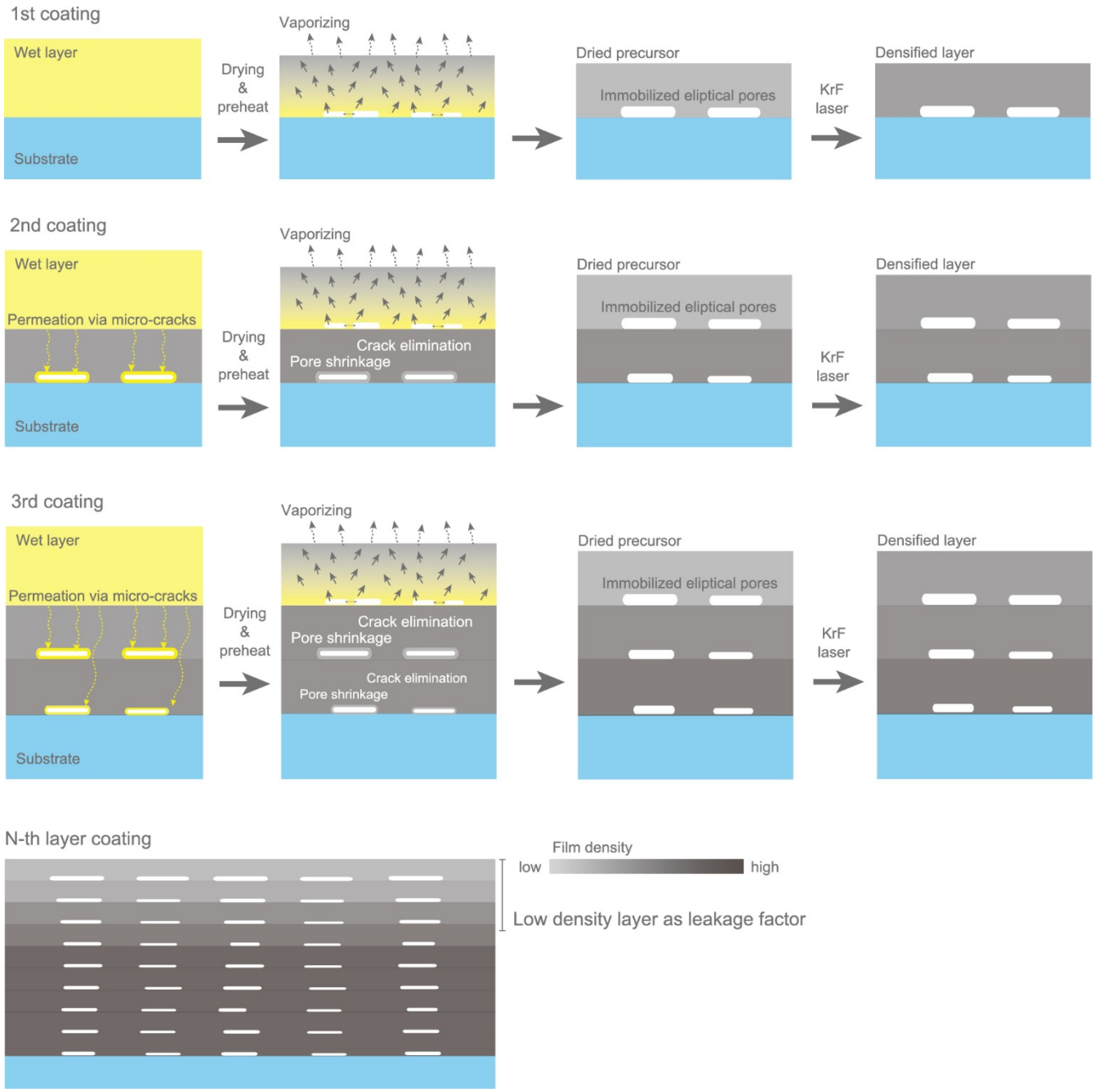

Fig. S4: The schematic illustration for the formations of elliptical pores during the multiple coating process.

Hard cracks in the YP prepared by nanoparticles deposition without laser irradiation

Fig. S5: The photographs of YP and Y4.

Surface morphology

The effects of laser fluence intensity on surface morphology and surface roughness were evaluated using a laser microscope (OPTELICS Hybrid^{+}, Lasertec) and FESEM.

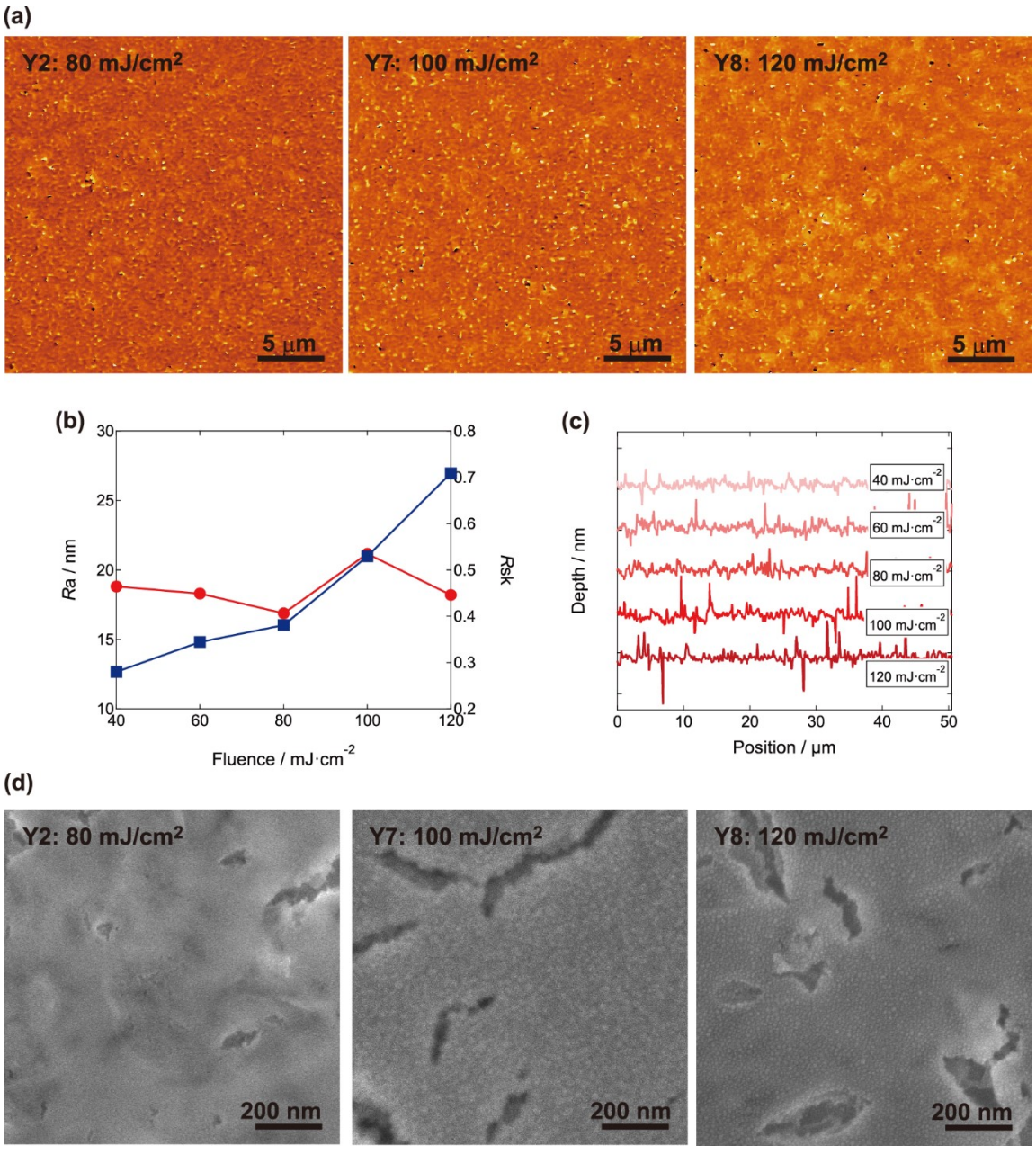

Fig. S6: (a) The surface morphology taken by laser microscope for Y2, Y7 and Y8. (b) The laser fluence dependence of (b) R_a and R_{sk} and (c) line profiles of height for the yttria films (Y2 and Y5–Y8). (d) The surface FESEM images for Y2, Y7 and Y8.

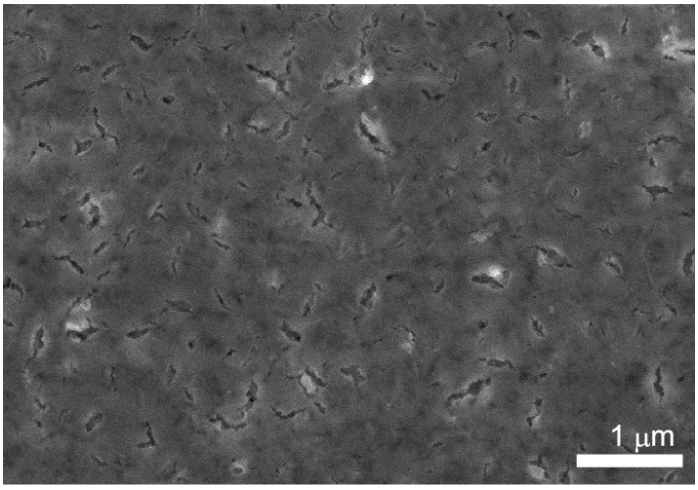

Fig. S7: The surface FESEM image of Y1.

References

S1. J. Iwasawa, R. Nishimizu, M. Tokita, M. Kiyohara and K. Uematsu, *J. Ceram. Soc. Japan*, 2006, **114**, 272–276.

S2. N. Boysen, D. Zanders, D. Rogalla, C. Bock, T. Berning, S. M. J. Beer and A. Devi, RSC Adv., 2021, 11, 2565–2574.

S3. L. Mai, N. Boysen, E. Subaşi, T. D. L. Arcos, D. Rogalla, G. Grundmeier, C. Bock, H. Lu and A. Devi, RSC Adv., 2018, 8, 4987–4994.

S4. P. De Rouffignac, J. Park and R. G. Gordon, *Chem. Mater.*, 2005, **17**, 4808–4814.

S5. C. Durand, C. Vallée, V. Loup, O. Salicio, C. Dubourdieu, S. Blonkowski, M. Bonvalot, P. Holloger and O. Joubert, *J. Vac. Sci. Technol. A Vacuum, Surfaces, Film.*, 2004, **22**, 655–660.

S6. C. Durand, C. Dubourdieu, C. Vallée, V. Loup, M. Bonvalot, H. Roussel, O. Renault, C. Durand, C. Dubourdieu, C. Vallée, V. Loup and M. Bonvalot, *J. Appl. Phys.*, 2004, **96**, 1719–1729.

S7. B. S. Karle, V. Dang, M. Prenzel, D. Rogalla, H. Becker and A. Devi, *Chem. Vap. Depos.*, 2015, **21**, 1–8.

S8. http://www.cvd.co.jp/wp/wp-content/uploads/2020/11/CVD_yttria_Physical_property_TCS.pdf

S9. H. J. Quah, W. F. Lim, S. C. Wimbush, Z. Lockman and K. Y. Cheong, *Electrochem. Solid-State Lett.*, 2010, **13**, H396–H398.

S10. C. K. Lee, W. S. Kim, H. Park, H. Jeon and H. Y. Pae, *Thin Solid Films*, 2005, **473**, 335–339.

S11. P. S. Das and A. Biswas, *Thin Solid Films*, 2011, **520**, 47–52.

S12. J. J. Araiza, M. A. Aguilar-Frutis and C. Falcony, *J. Vac. Sci. Technol. B*, 2001, **19**, 2206–2211.

S13. A. Liu, G. Liu, H. Zhu, Y. Meng, H. Song, B. Shin, E. Fortunato, R. Martins and F. Shan, *Curr. Appl. Phys.*, 2015, **15**, S75–S81.

S14. S. Choi, B. Park, S. Jeong and H. Jung, *Electrochem. Solid-State Lett.*, 2011, **14**, H426–H429.

S15. H. Xu, X. Ding, J. Qi, X. Yang and J. Zhang, *Coatings*, 2021, **11**, 969.

S16. J. Song, E. Choi, S. Oh, J. So, S. Lee, J. Kim and J. Yun, *Ceram. Int.*, 2019, **45**, 22169–22174.

S17. T. Lin, D. Wuu, S. Huang and W. Wang, *Japanease J. Appl. Phys.*, 2016, **55**, 126201.

S18. J. Kitamura, H. Ibe, F. Yuasa and H. Mizuno, *J. Therm. Spray Technol.*, 2008, **17**, 878–886.

S19. J. Kotlan, R. C. Seshadri, S. Sampath, P. Ctibor, Z. Pala and R. Musalek, *Ceram. Int.*, 2015, **41**, 11169–11176.

S20. J. Leng, Z. Yu, Y. Li, D. Zhang, X. Liao and W. Xue, *Appl. Surf. Sci.*, 2010, **256**, 5832–5836.

S21. V. Mikhaelashvili, Y. Betzer, I. Prudnikov, M. Orenstein, D. Ritter and G. Eisenstein, *J. Appl. Phys.*, 1998, **84**, 6747–6752.

S22. A. C. Rastogi and R. N. Sharma, *J. Appl. Phys.*, 1992, **71**, 5041–5052.

S23. V. Ioannou-Sougleridis, G. Vellianitis and A. Dimoulas, *J. Appl. Phys.*, 2003, **93**, 3982–3989.

S24. S. Karle, V-S. Dang, M. Prenzel, D. Rogalla, H-W. Becker and A. Devi, Chem. Vap. Deposition 2015, **21**, 335–342.

S25. V. Swamy, H. J. Seifert and F. Aldinger, J. Alloys Compd. 1998, **269**, 201–207.

S26. T. Nakajima and T. Tsuchiya, J. Mater. Chem. C, 2015, **3**, 3809–3816.